Relativistic energy density functionals: Low-energy collective states of 240Pu and 166Er

Li, Z. P.; Nikšić, Tamara; Vretenar, Dario; Ring, Peter; Meng, Jie

Relativistic energy density functionals: Low-energy collective states of ^{240}Pu and ^{166}Er

Z. P. Li,[1,2,5] T. Nikšić,[1] D. Vretenar,[1] P. Ring,[2,3] and J. Meng[2,4]

[1]*Physics Department, Faculty of Science, University of Zagreb, 10000 Zagreb, Croatia*
[2]*State Key Laboratory of Nuclear Physics and Technology, School of Physics, Peking University, Beijing 100871, China*
[3]*Physik-Department der Technischen Universität München, D-85748 Garching, Germany*
[4]*School of Physics and Nuclear Energy Engineering, Beihang University, Beijing 100191, China*
[5]*School of Physical Science and Technology, Southwest University, Chongqing 400715, China*

The empirical relativistic density-dependent, point-coupling energy density functional, adjusted exclusively to experimental binding energies of a large set of deformed nuclei with $A \approx$ 150–180 and $A \approx$ 230–250, is tested with spectroscopic data for ^{166}Er and ^{240}Pu. Starting from constrained self-consistent triaxial relativistic Hartree-Bogoliubov calculations of binding energy maps as functions of the quadrupole deformation in the β-γ plane, excitation spectra and $E2$ transition probabilities are calculated as solutions of the corresponding microscopic collective Hamiltonian in five dimensions for quadrupole vibrational and rotational degrees of freedom and compared with available data on low-energy collective states.

I. INTRODUCTION

The framework of nuclear energy density functionals (NEDFs) provides, at present, the most complete microscopic approach to the rich variety of structure phenomena in medium-heavy and heavy complex nuclei, including regions of the nuclide chart far from the valley of β stability [1,2]. By employing global functionals parametrized by a set of $\approx$10 coupling constants, the current generation of EDF-based models has achieved a high level of accuracy in the description of ground states and properties of excited states, exotic unstable nuclei, and even nuclear systems at the nucleon drip lines.

The exact energy density functional, which in principle includes all higher-order correlations, is approximated by a functional of powers and gradients of ground-state nucleon densities and currents, representing distributions of matter, spins, momentum, and kinetic energy. Although it models the effective interaction between nucleons, a general density functional is not necessarily related to any given NN potential and, in fact, some of the most successful modern functionals are entirely empirical. However, it would clearly be desirable to have a fully microscopic foundation for a universal EDF framework, starting from a Hamiltonian that describes two-nucleon and few-body scattering and bound-state observables. Important advances in this direction have been made in recent years and, for the framework of nonrelativistic EDFs, we refer the reader to the recent review of Ref. [3]. Relativistic microscopic EDFs were developed based on a perturbative chiral effective field theory approach to nuclear matter [4,5], thus establishing connections with chiral dynamics and the symmetry-breaking pattern of low-energy QCD.

However, even if a fully microscopic energy density functional is eventually developed, the parameters of that functional would still have to be fine-tuned to structure data of finite nuclei. This is because data on nucleon-nucleon scattering and few-nucleon systems, or gross properties of infinite nuclear matter, cannot determine the density functional to the level of accuracy necessary for a quantitative description of medium-heavy and heavy nuclei. Most empirical and semimicroscopic functionals have been adjusted to a relatively small set of spherical closed-shell nuclei, because these systems are easy to calculate and can simply be included in multiparameter least-squares fits. It should be noted, however, that ground-state data of closed-shell nuclei include long-range correlations that cannot be absorbed into global functionals. It is well known that energy density functionals, or, at the level of practical application, self-consistent mean-field models, provide a much better description of deformed, open-shell nuclei. Therefore, in a recent work [6], we took a different approach and adjusted an empirical relativistic density functional directly to experimental binding energies of a large set of axially deformed nuclei. Starting from microscopic nucleon self-energies in nuclear matter, and empirical global properties of the nuclear matter equation of state, the coupling parameters of the functional were determined in a careful comparison of the predicted binding energies with data, for a set of 64 axially deformed nuclei in the mass regions $A \approx$ 150–180 and $A \approx$ 230–250. The resulting functional, which we denote DD-PC1 (for density-dependent, point-coupling), was further tested in a series of illustrative calculations of properties of spherical and deformed medium-heavy and heavy nuclei, including binding energies, charge radii, deformation parameters, neutron skin thickness, and excitation energies of giant multipole resonances.

Relativistic energy density functionals, in particular, have mostly been applied at the self-consistent mean-field level. For EDF-based models to make detailed predictions of excitation spectra and electromagnetic transition rates, symmetries broken by the static nuclear mean field (translational, rotational, and particle number) must be restored, and fluctuations around the mean-field minimum must be taken into account. This can only be achieved in a consistent framework in which symmetry restoration and configuration mixing calculations are performed. While most of these "beyond mean-field methods" have routinely been applied with nonrelativistic

density functionals for many years, it is only more recently that multireference calculations have been reported using relativistic density functionals [7–10]. The relativistic functional DD-PC1 was adjusted only to experimental binding energies in two mass regions and tested in mean-field calculations of ground-state nuclear properties. It would, therefore, be important to further test this functional in comparison with spectroscopic data. In this work we take a first step in this direction and calculate low-energy collective excitation spectra and $E2$ transition probabilities for two nuclei in the same mass regions in which the parameters of DD-PC1 have been adjusted to binding energies: ^{166}Er and ^{240}Pu.

In Sec. II we include a brief outline of the relativistic energy density functional DD-PC1. Section III describes our theoretical framework: the three-dimensional relativistic Hartree-Bogoliubov model with a separable pairing force that is used to map the energy surface as a function of quadrupole deformation, and the model for the solution of a collective Hamiltonian in five dimensions for quadrupole vibrational and rotational degrees of freedom. The positive-parity low-energy collective states of ^{240}Pu and ^{166}Er are calculated and compared with available data in Sec. IV. Section V summarizes the results and presents an outlook for future studies.

II. THE RELATIVISTIC DENSITY FUNCTIONAL DD-PC1

The basic building blocks of a relativistic nuclear energy density functional are the densities and currents bilinear in the Dirac spinor field ψ of the nucleon: $\bar{\psi}\mathcal{O}_\tau\Gamma\psi$, with $\mathcal{O}_\tau \in \{1, \tau_i\}$ and $\Gamma \in \{1, \gamma_\mu, \gamma_5, \gamma_5\gamma_\mu, \sigma_{\mu\nu}\}$. Here τ_i are the isospin Pauli matrices and Γ generically denotes the Dirac matrices. The nuclear ground-state density and energy are determined by the self-consistent solution of linear relativistic single-nucleon Kohn-Sham equations. To derive those equations it is useful to construct an interaction Lagrangian with four-fermion (contact) interaction terms in the various isospace-space channels: isoscalar-scalar $(\bar{\psi}\psi)^2$, isoscalar-vector $(\bar{\psi}\gamma_\mu\psi)(\bar{\psi}\gamma^\mu\psi)$, isovector-scalar $(\bar{\psi}\vec{\tau}\psi)\cdot(\bar{\psi}\vec{\tau}\psi)$, and isovector-vector $(\bar{\psi}\vec{\tau}\gamma_\mu\psi)\cdot(\bar{\psi}\vec{\tau}\gamma^\mu\psi)$. A general Lagrangian can be written as a power series in the currents $\bar{\psi}\mathcal{O}_\tau\Gamma\psi$ and their derivatives, with higher-order terms representing in-medium many-body correlations. The Lagrangian that corresponds to the functional DD-PC1 [6] includes second-order interaction terms, with many-body correlations (short-distance correlations, as well as intermediate and long-range dynamics), encoded in density-dependent coupling functions:

$$\begin{aligned}
\mathcal{L} = {} & \bar{\psi}(i\gamma\cdot\partial - m)\psi - \frac{1}{2}\alpha_S(\hat{\rho}_v)(\bar{\psi}\psi)(\bar{\psi}\psi) \\
& - \frac{1}{2}\alpha_V(\hat{\rho}_v)(\bar{\psi}\gamma^\mu\psi)(\bar{\psi}\gamma_\mu\psi) - \frac{1}{2}\alpha_{TV}(\hat{\rho}_v)(\bar{\psi}\vec{\tau}\gamma^\mu\psi) \\
& \times (\bar{\psi}\vec{\tau}\gamma_\mu\psi) - \frac{1}{2}\delta_S(\partial_\nu\bar{\psi}\psi)(\partial^\nu\bar{\psi}\psi) \\
& - e\bar{\psi}\gamma\cdot A\frac{(1-\tau_3)}{2}\psi.
\end{aligned} \quad (1)$$

In addition to the free-nucleon Lagrangian and the point-coupling interaction terms, when applied to nuclei, the model

must include the coupling of the protons to the electromagnetic field. The derivative term in Eq. (1) accounts for leading effects of finite-range interactions that are crucial for a quantitative description of nuclear density distribution (e.g., nuclear radii). Equation (1) includes only one isovector term (i.e., the isovector-vector interaction) because, although the isovector strength has a relatively well-defined value, the distribution between the scalar and vector channels is not determined by ground-state data.

The strength parameters of the interaction terms in Eq. (1) are, in general, functions of $\sqrt{j^\mu j_\mu}$, with the nucleon four-current: $j^\mu = \bar{\psi}\gamma^\mu\psi = \hat{\rho}_v u^\mu$. The four-velocity u^μ is defined as $(1 - \mathbf{u}^2)^{-1/2}(1, \mathbf{u})$. However, at velocities relevant for this investigation, $\mathbf{u} \approx 0$ in the nuclear rest frame and thus the parameters depend only on the baryon density $\hat{\rho}_v = \psi^\dagger\psi$. The single-nucleon Dirac equation, the relativistic analog of the Kohn-Sham equation, is obtained from the variation of the Lagrangian with respect to $\bar{\psi}$,

$$\left[\gamma_\mu\left(i\partial^\mu - \Sigma^\mu - \Sigma_R^\mu\right) - (m + \Sigma_S)\right]\psi = 0, \quad (2)$$

with the nucleon self-energies defined by the following relations:

$$\Sigma^\mu = \alpha_V(\rho_v)j^\mu + e\frac{(1-\tau_3)}{2}A^\mu, \quad (3)$$

$$\Sigma_R^\mu = \frac{1}{2}\frac{j^\mu}{\rho_v}\left\{\frac{\partial\alpha_S}{\partial\rho}\rho_s^2 + \frac{\partial\alpha_V}{\partial\rho}j_\mu j^\mu + \frac{\partial\alpha_{TV}}{\partial\rho}\vec{j}_\mu\vec{j}^\mu\right\}, \quad (4)$$

$$\Sigma_S = \alpha_S(\rho_v)\rho_s - \delta_S\Box\rho_s, \quad (5)$$

$$\Sigma_{TV}^\mu = \alpha_{TV}(\rho_v)\vec{j}^\mu. \quad (6)$$

In addition to the contributions of the isoscalar-vector four-fermion interaction and the electromagnetic interaction, the isoscalar-vector self-energy Σ^μ includes the "rearrangement" terms Σ_R^μ, arising from the variation of the vertex functionals α_S, α_V, and α_{TV} with respect to the nucleon fields in the vector density operator $\hat{\rho}_v$.

On the mean-field level, the nuclear ground state $|\phi_0\rangle$ is represented by the self-consistent solution of the system of equations (2)–(6), with the isoscalar and isovector four-currents and scalar density:

$$j_\mu = \langle\phi_0|\bar{\psi}\gamma_\mu\psi|\phi_0\rangle = \sum_{k=1}^N v_k^2\bar{\psi}_k\gamma_\mu\psi_k, \quad (7)$$

$$\vec{j}_\mu = \langle\phi_0|\bar{\psi}\gamma_\mu\vec{\tau}\psi|\phi_0\rangle = \sum_{k=1}^N v_k^2\bar{\psi}_k\gamma_\mu\vec{\tau}\psi_k, \quad (8)$$

$$\rho_s = \langle\phi_0|\bar{\psi}\psi|\phi_0\rangle = \sum_{k=1}^N v_k^2\bar{\psi}_k\psi_k, \quad (9)$$

where ψ_k are Dirac spinors, and the sum runs over occupied positive-energy single-nucleon orbitals, including the corresponding occupation factors v_k^2. The single-nucleon Dirac equations are solved self-consistently in the "no-sea" approximation that omits the explicit contribution of negative-energy solutions of the relativistic equations to the densities and currents.

TABLE I. Parameters of the relativistic energy density functional DD-PC1 [cf. Eq. (10)].[a]

Parameter	Value
a_S (fm^2)	-10.0462
b_S (fm^2)	-9.1504
c_S (fm^2)	-6.4273
d_S	1.3724
a_V (fm^2)	5.9195
b_V (fm^2)	8.8637
d_V	0.6584
b_{TV} (fm^2)	1.8360
d_{TV}	0.6403
δ_S (fm^4)	-0.8149

[a]The nucleon mass is $m = 939$ MeV.

The strength and density dependence of the interaction terms of the Lagrangian Eq. (1) are parametrized as follows [6]:

$$\alpha_S(\rho) = a_S + (b_S + c_S x)e^{-d_S x},$$
$$\alpha_V(\rho) = a_V + b_V e^{-d_V x}, \qquad (10)$$
$$\alpha_{TV}(\rho) = b_{TV} e^{-d_{TV} x},$$

where $x = \rho/\rho_{\text{sat}}$, and ρ_{sat} denotes the nucleon density at saturation in symmetric nuclear matter. The set of 10 parameters was adjusted in a multistep parameter fit exclusively to the experimental masses of 64 axially deformed nuclei in the mass regions $A \approx 150$–180 and $A \approx 230$–250. The resulting functional DD-PC1 was further tested in calculations of binding energies, charge radii, deformation parameters, neutron skin thickness, and excitation energies of giant monopole and dipole resonances. The nuclear matter equation of state, corresponding to DD-PC1, is characterized by the following properties at the saturation point: nucleon density $\rho_{\text{sat}} = 0.152$ fm^{-3}, volume energy $a_v = -16.06$ MeV, surface energy $a_s = 17.498$ MeV, symmetry energy $a_4 = 33$ MeV, and the nuclear matter compression modulus $K_{\text{nm}} = 230$ MeV. The parameters of DD-PC1 are given in Table I.

III. THEORETICAL FRAMEWORK: COLLECTIVE HAMILTONIAN IN FIVE DIMENSIONS

A. Three-dimensional relativistic Hartee-Bogoliubov model with a separable pairing interaction

The relativistic Hartee-Bogoliubov (RHB) model [11–13] provides a unified description of particle-hole (ph) and particle-particle (pp) correlations on a mean-field level by combining two average potentials: the self-consistent mean field that encloses all the long-range ph correlations, and a pairing field $\hat{\Delta}$ which sums up the pp correlations. In the present analysis the mean-field potential is determined by the relativistic density functional DD-PC1 [6] in the ph channel, and a new separable pairing interaction, recently introduced in Refs. [14–16], is used in the pp channel.

In the RHB framework, the nuclear single-reference state is described by a generalized Slater determinant $|\Phi\rangle$ that represents the vacuum with respect to independent quasiparticles. The quasiparticle operators are defined by the unitary Bogoliubov transformation, and the corresponding Hartree-Bogoliubov wave functions U and V are determined by the solution of the RHB equation. In coordinate representation,

$$\begin{pmatrix} h_D - m - \lambda & \Delta \\ -\Delta^* & -h_D^* + m + \lambda \end{pmatrix} \begin{pmatrix} U_k(r) \\ V_k(r) \end{pmatrix} = E_k \begin{pmatrix} U_k(r) \\ V_k(r) \end{pmatrix} \tag{11}$$

In the relativistic case the self-consistent mean field corresponds to the single-nucleon Dirac Hamiltonian $\hat{h}_D$ of Eq. (2); U and V are Dirac spinors.

The pairing force is separable in momentum space: $\langle k|V^{1S_0}|k'\rangle = -Gp(k)p(k')$ [14–16]. By assuming a simple Gaussian ansatz $p(k) = e^{-a^2 k^2}$, the two parameters G and a were adjusted to reproduce the density dependence of the gap at the Fermi surface in nuclear matter, calculated with a Gogny force. For the D1S parametrization of the Gogny force [17], the corresponding parameters of the separable pairing interaction take the following values: $G = -728$ MeV fm^3 and $a = 0.644$ fm. When transformed from momentum to coordinate space, the force takes the form

$$V(\boldsymbol{r}_1, \boldsymbol{r}_2, \boldsymbol{r}_1', \boldsymbol{r}_2') = G\delta(\boldsymbol{R} - \boldsymbol{R}')P(\boldsymbol{r})P(\boldsymbol{r}')\tfrac{1}{2}(1 - P^\sigma), \tag{12}$$

where $\boldsymbol{R} = \frac{1}{2}(\boldsymbol{r}_1 + \boldsymbol{r}_2)$ and $\boldsymbol{r} = \boldsymbol{r}_1 - \boldsymbol{r}_2$ denote the center-of-mass and the relative coordinates, and $P(\boldsymbol{r})$ is the Fourier transform of $p(k)$:

$$P(\boldsymbol{r}) = \frac{1}{(4\pi a^2)^{3/2}} e^{-\boldsymbol{r}^2/4a^2}. \tag{13}$$

The pairing force is of finite range and, because of the presence of the factor $\delta(\boldsymbol{R} - \boldsymbol{R}')$, it preserves translational invariance. Even though $\delta(\boldsymbol{R} - \boldsymbol{R}')$ implies that this force is not completely separable in coordinate space, the corresponding pp matrix elements can be represented as a sum of a finite number of separable terms in the basis of a three-dimensional (3D) harmonic oscillator. The force Eq. (12) reproduces pairing properties of spherical and axially deformed nuclei calculated with the original Gogny force, but with the important advantage that the computational cost is greatly reduced.

To describe nuclei with general triaxial shapes, the Dirac-Hartree-Bogoliubov equations (11) are solved by expanding the nucleon spinors in the basis of a 3D harmonic oscillator in Cartesian coordinates. In the present calculation the basis includes $N_f^{\max} = 14$ major oscillator shells for the nucleus ^{166}Er, and $N_f^{\max} = 16$ for ^{240}Pu. The map of the energy surface as a function of the quadrupole deformation is obtained by imposing constraints on the axial and triaxial quadrupole moments. The method of quadratic constraint uses an unrestricted variation of the function

$$\langle \hat{H} \rangle + \sum_{\mu=0,2} C_{2\mu}(\langle \hat{Q}_{2\mu} \rangle - q_{2\mu})^2, \tag{14}$$

where $\langle \hat{H} \rangle$ is the total energy, and $\langle \hat{Q}_{2\mu} \rangle$ denotes the expectation value of the mass quadrupole operators:

$$\hat{Q}_{20} = 2z^2 - x^2 - y^2 \quad \text{and} \quad \hat{Q}_{22} = x^2 - y^2. \tag{15}$$

The variable $q_{2\mu}$ is the constrained value of the multipole moment, and $C_{2\mu}$ is the corresponding stiffness constant [18].

B. Collective Hamiltonian in five dimensions

The self-consistent solutions of the constrained triaxial RHB equations (i.e., the single-quasiparticle energies and wave functions for the entire energy surface as functions of the quadrupole deformation), provide the microscopic input for the parameters of a collective Hamiltonian for quadrupole vibrational and rotational degrees of freedom [9]. The five quadrupole collective coordinates are parametrized in terms of two deformation parameters β and γ, and three Euler angles $(\phi, \theta, \psi) \equiv \Omega$, which define the orientation of the intrinsic principal axes in the laboratory frame:

$$\hat{H} = \hat{T}_{\text{vib}} + \hat{T}_{\text{rot}} + V_{\text{coll}}, \tag{16}$$

with the vibrational kinetic energy

$$
\begin{aligned}
\hat{T}_{\text{vib}} = -\frac{\hbar^2}{2\sqrt{wr}} &\left[\frac{1}{\beta^4} \left(\frac{\partial}{\partial \beta} \sqrt{\frac{r}{w}} \beta^4 B_{\gamma\gamma} \frac{\partial}{\partial \beta} \right.\right. \\
&\left. - \frac{\partial}{\partial \beta} \sqrt{\frac{r}{w}} \beta^3 B_{\beta\gamma} \frac{\partial}{\partial \gamma} \right) \\
&+ \frac{1}{\beta \sin 3\gamma} \left(-\frac{\partial}{\partial \gamma} \sqrt{\frac{r}{w}} \sin 3\gamma\, B_{\beta\gamma} \frac{\partial}{\partial \beta} \right. \\
&\left.\left. + \frac{1}{\beta} \frac{\partial}{\partial \gamma} \sqrt{\frac{r}{w}} \sin 3\gamma\, B_{\beta\beta} \frac{\partial}{\partial \gamma} \right) \right],
\end{aligned}
\tag{17}
$$

rotational kinetic energy

$$\hat{T}_{\text{rot}} = \frac{1}{2} \sum_{k=1}^{3} \frac{\hat{J}_k^2}{\mathcal{I}_k}, \tag{18}$$

and V_{coll} is the collective potential. The variable $\hat{J}_k$ denotes the components of the angular momentum in the body-fixed frame of a nucleus, and the mass parameters $B_{\beta\beta}$, $B_{\beta\gamma}$, and $B_{\gamma\gamma}$, as well as the moments of inertia $\mathcal{I}_k$, depend on the quadrupole deformation variables β and γ:

$$\mathcal{I}_k = 4 B_k \beta^2 \sin^2(\gamma - 2k\pi/3). \tag{19}$$

Two additional quantities that appear in the expression for the vibrational energy, $r = B_1 B_2 B_3$ and $w = B_{\beta\beta} B_{\gamma\gamma} - B_{\beta\gamma}^2$, determine the volume element in the collective space.

The dynamics of the collective Hamiltonian is governed by the seven functions of the intrinsic deformations β and γ: the collective potential, the three mass parameters $B_{\beta\beta}$, $B_{\beta\gamma}$, $B_{\gamma\gamma}$, and the three moments of inertia, $\mathcal{I}_k$. These functions are determined by the microscopic nuclear energy density functional and the effective interaction in the pp channel. The moments of inertia are calculated from the Inglis-Belyaev formula:

$$\mathcal{I}_k = \sum_{i,j} \frac{|\langle ij|\hat{J}_k|\Phi\rangle|^2}{E_i + E_j} \quad k = 1, 2, 3, \tag{20}$$

where k denotes the axis of rotation, the summation runs over proton and neutron quasiparticle states $|ij\rangle = \beta_i^\dagger \beta_j^\dagger |\Phi\rangle$, and $|\Phi\rangle$ represents the quasiparticle vacuum. The mass parameters associated with the two quadrupole collective coordinates $q_0 = \langle \hat{Q}_{20} \rangle$ and $q_2 = \langle \hat{Q}_{22} \rangle$ are calculated in the cranking approximation:

$$B_{\mu\nu}(q_0, q_2) = \frac{\hbar^2}{2} \left[\mathcal{M}_{(1)}^{-1} \mathcal{M}_{(3)} \mathcal{M}_{(1)}^{-1} \right]_{\mu\nu}, \tag{21}$$

with

$$\mathcal{M}_{(n),\mu\nu}(q_0, q_2) = \sum_{i,j} \frac{|\langle \Phi | \hat{Q}_{2\mu} | ij \rangle \langle ij | \hat{Q}_{2\nu} | \Phi \rangle|}{(E_i + E_j)^n}. \tag{22}$$

Finally, the potential V_{coll} in the collective Hamiltonian Eq. (16) is obtained by subtracting the zero-point energy corrections from the total energy that corresponds to the solution of constrained RHB equations, at each point on the triaxial deformation plane [9].

The Hamiltonian Eq. (16) describes quadrupole vibrations, rotations, and the coupling of these collective modes. The corresponding eigenvalue problem is solved using an expansion of eigenfunctions in terms of a complete set of basis functions that depend on the deformation variables β and γ, and the Euler angles ϕ, θ, and ψ [9]. The diagonalization of the Hamiltonian yields the excitation energies and collective wave functions:

$$\Psi_\alpha^{IM}(\beta, \gamma, \Omega) = \sum_{K \in \Delta I} \psi_{\alpha K}^I(\beta, \gamma) \Phi_{MK}^I(\Omega). \tag{23}$$

The angular part corresponds to linear combinations of Wigner functions

$$\Phi_{MK}^I(\Omega) = \sqrt{\frac{2I+1}{16\pi^2(1+\delta_{K0})}} \left[D_{MK}^{I*}(\Omega) + (-1)^I D_{M-K}^{I*}(\Omega) \right], \tag{24}$$

and the summation in Eq. (23) is over the allowed set of K values:

$$\Delta I = \begin{cases} 0, 2, \ldots, I & \text{for } I \bmod 2 = 0, \\ 2, 4, \ldots, I-1 & \text{for } I \bmod 2 = 1. \end{cases} \tag{25}$$

Using the collective wave functions of Eq. (23), various observables can be calculated and compared with experimental results. For instance, the quadrupole $E2$ reduced transition probability is

$$B(E2;\ \alpha I \to \alpha' I') = \frac{1}{2I+1} |\langle \alpha' I' || \hat{\mathcal{M}}(E2) || \alpha I \rangle|^2, \tag{26}$$

where $\hat{\mathcal{M}}(E2)$ is the electric quadrupole operator. For the $\hat{\mathcal{M}}(E2)$ matrix elements, the current implementation of the model uses a local expression in the collective deformation variables [19]. This approximation is justified in the case of large overlaps between different vibrational amplitudes [20], but it may be less suited for transitions between states with a rather small overlap (e.g., for transitions between superdeformed bands and bands at normal deformation).

IV. TEST OF DD-PC1 IN TWO MASS REGIONS

A. ^{240}Pu at normal and superdeformation

The structure of the nucleus ^{240}Pu and its double-humped fission barrier has become a standard benchmark for models based on the self-consistent mean-field approach and the corresponding effective interactions or density functionals.

Numerous theoretical studies of this nucleus are reported in the literature; here we only mention the most recent ones that are also relevant for the present analysis. In their review of self-consistent mean-field models for nuclear structure [1], which also contains an extensive list of references to previous studies of fission barriers using mean-field-based models, Bender *et al.* compared paths in the deformation energy landscape of ^{240}Pu obtained with various Skyrme, Gogny, and relativistic mean-field (RMF) interactions. In general, relaxing constraints on symmetries lowers the fission barriers. The predicted shapes are triaxial and reflection symmetric at the first barrier around $\beta \approx 0.6$, and they are axial and reflection asymmetric at the second barrier, located around $\beta \approx 1.3$. The systematics of axially symmetric fission barriers in Th, U, Pu, Cm, and Cf nuclei, as well as for superheavy elements $Z = 108$–120, using several Skyrme and RMF interactions, was investigated in Ref. [21]. The fission barriers of 26 even-Z nuclei with $Z = 90$–102, up to and beyond the second saddle point, were calculated in Ref. [22] with the constrained Hartree-Fock approach based on the Skyrme effective interaction SkM*. The fission barriers of ^{240}Pu beyond the second saddle point were also explored using the axially quadrupole constrained RMF model with the PK1 effective interaction [23].

A number of studies were also reported that include beyond mean-field methods (i.e., multireference calculations that explored the effects of symmetry restoration and configuration mixing). Among the more recent, in Ref. [24] $\pi = +$ collective quadrupole levels and $\pi = \pm$ two-quasiparticle (2qp) excitations in even-even Th, U, Pu, and Cm isotopes were investigated at normal and superdeformed shapes in microscopic calculations based on the Gogny force. Collective levels were obtained from axial and triaxial constrained Hartree-Fock-Bogoliubov (HFB) and configuration mixing calculations, whereas blocking calculations were performed for 2qp states. Starting from axially constrained Hartree-Fock + BCS wave functions obtained with the Skyrme interactions Sly4 and Sly6, the study of Ref. [25] examined the influence of exact angular momentum projection and configuration mixing on the structure (the deformation energy curve, and properties of rotational bands at normal and superdeformation) of ^{240}Pu. An extensive analysis of structure properties of 55 even-even actinides at normal and isomeric potential deformations was carried out in Ref. [26]. Based on HFB calculations with the Gogny D1S force, with constraints on axial and triaxial quadrupole deformations, shape isomers and $\pi = +$ vibrations were obtained as solutions of the five-dimensional collective Hamiltonian, and spin isomers were analyzed in the blocking approximation. Model predictions were shown to be in very good agreement with data on multipole moments, moments of inertia, spin and shape isomers, inner and outer potential barrier heights, and shape isomer lifetimes. Properties of collective quadrupole states of transactinide nuclei and, in particular, superdeformed collective states in the second minimum of ^{240}Pu were recently studied using a five-dimensional collective Hamiltonian based on the adiabatic time-dependent HFB approach with the Skyrme forces SkM*, SIII, and SLy4 [27].

In Fig. 1 we display the RHB triaxial quadrupole binding energy map of ^{240}Pu in the β-γ plane ($0 \leqslant \gamma \leqslant 60°$), calculated with the DD-PC1 energy density functional plus the

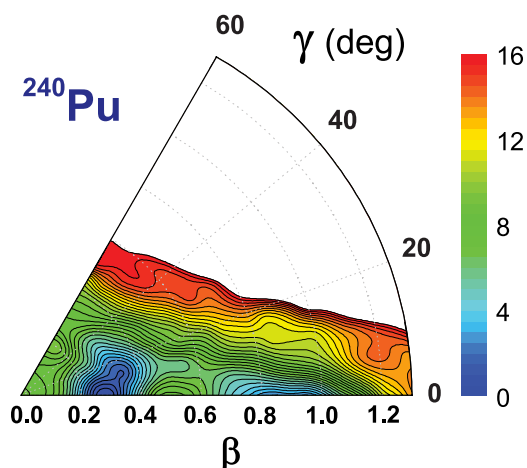
FIG. 1. (Color online) Self-consistent RHB triaxial quadrupole binding energy maps of ^{240}Pu in the β-γ plane ($0 \leqslant \gamma \leqslant 60°$). All energies are normalized with respect to the binding energy of the absolute minimum. The contours join points on the surface with the same energy (in MeV).

pairing interaction Eq. (12). The calculation was carried out on a mesh of quadrupole deformation parameters with $\Delta\beta = 0.05$ and $\Delta\gamma = 6°$. All energies are normalized with respect to the binding energy of the absolute minimum, and the contours join points on the surface with the same energy (in MeV). Because the present implementation of the model does not include reflection-asymmetric shapes, the potential energy surface (PES) is calculated only up to $\beta \leqslant 1.3$. For larger deformations (i.e., in the region of the second barrier), octupole deformations should be taken into account. The absolute minimum is calculated at $\beta = 0.28$, $\gamma = 0°$, and a second (superdeformed) valley is predicted around $\beta \approx 0.9$. The axially symmetric barrier at $\beta \approx 0.5$ is bypassed through the triaxial region, bringing the height of the barrier much closer to the empirical value. This is shown more clearly in Fig. 2, where we plot the deformation energy curves and the inner barrier of ^{240}Pu as functions of the axial deformation β. The two curves correspond to the axially symmetric RHB calculation (solid curve), and to the projection on the β-axis of the triaxial PES (dashed curve). The experimental values for the ground-state deformation, the barrier height, and the energy of the second minimum are taken from Refs. [28–31]. One might notice a very good agreement between theory and available data. In particular, the inclusion of triaxial shapes lowers the inner barrier by ≈ 2 MeV. Similar results were also obtained in constrained self-consistent mean-field calculations using Skyrme functionals [1], and in the HFB + Gogny analysis of the actinide region [26] it was shown that the inner barriers of the actinides were systematically lowered by up to 4 MeV when calculations included triaxial shapes.

Starting from constrained self-consistent solutions of the RHB equations (i.e., employing single-quasiparticle energies and wave functions that correspond to each point on the energy surface shown in Fig. 1), the parameters that determine the collective Hamiltonian—the mass parameters $B_{\beta\beta}$, $B_{\beta\gamma}$, and $B_{\gamma\gamma}$, the three moments of inertia $\mathcal{I}_k$, as well as the zero-point energy corrections—are calculated as functions of the deformations
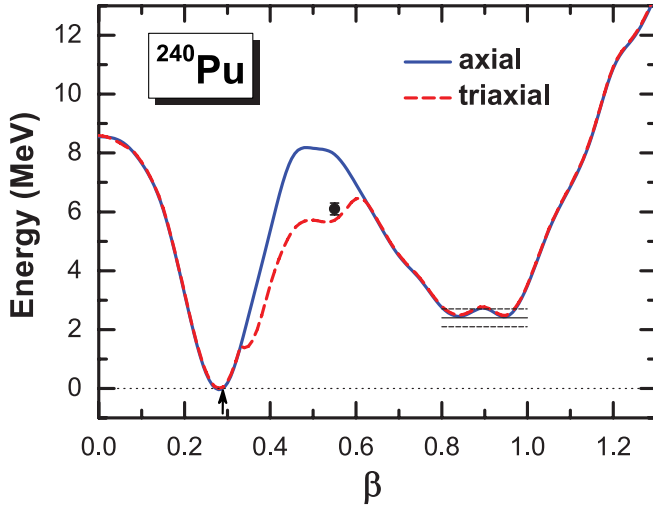
FIG. 2. (Color online) Deformation energy curves and the inner barrier of ^{240}Pu as functions of the axial deformation β. The two curves correspond to the axially symmetric RHB calculation (solid line) and to the projection on the β axis of the triaxial PES (dashed line), calculated with the functional DD-PC1. The experimental values for the ground-state deformation, the barrier height, and the energy of the second minimum are indicated with an arrow, a symbol with error bars, and three lines indicating the value and its errors, respectively. The data are taken from Refs. [28–31].

β and γ. The excitation spectrum of collective states is obtained by diagonalization of the resulting Hamiltonian. In Fig. 3 the calculated low-energy spectrum of ^{240}Pu is compared to data for the three lowest positive-parity bands at normal

deformation, and the lowest $\pi = +$ superdeformed band. In addition to the yrast ground-state band, in deformed and transitional nuclei, excited states are also assigned to (quasi) β and γ bands. This is done according to the distribution of the projection K of the angular momentum I on the z axis of the body-fixed frame:

$$N_K = 6 \int_0^{\pi/3} \int_0^\infty |\psi_{\alpha,K}^I(\beta, \gamma)|^2 \beta^4 |\sin 3\gamma| \, d\beta \, d\gamma, \quad (27)$$

where the components $\psi_{\alpha,K}^I(\beta, \gamma)$ are defined in Eq. (23). For large deformations, the K quantum number is to a good approximation conserved. Consequently, only one of the integrals of Eq. (27) will give a value close to 1. A broader distribution of N_K values in the state $|\alpha I\rangle$ provides a measure of the mixing of intrinsic configurations. Excited states with predominant $K = 2$ components in the wave function are assigned to the γ band, whereas the β band comprises the states above the yrast characterized by dominant $K = 0$ components. States $K = 0$ are assigned to the superdeformed band based on the calculated average value of the deformation parameter β:

$$\langle \beta \rangle_{I\alpha} = \sqrt{\langle \beta^2 \rangle_{I\alpha}}, \quad \text{where} \quad \langle \beta^2 \rangle_{I\alpha} = \langle \Psi_\alpha^I | \beta^2 | \Psi_\alpha^I \rangle. \quad (28)$$

We also verified that the rate of the $E0$ transition from the superdeformed band to the ground state is four orders of magnitude smaller than the rate of the corresponding transition from the bandhead of the β band.

For the moments of inertia of the collective Hamiltonian, we multiplied the Inglis-Belyaev (IB) values from Eq. (20) with a common factor determined in such a way that the calculated energy of the 2_1^+ state coincides with the experimental value. The additional scale parameter is necessary because of the
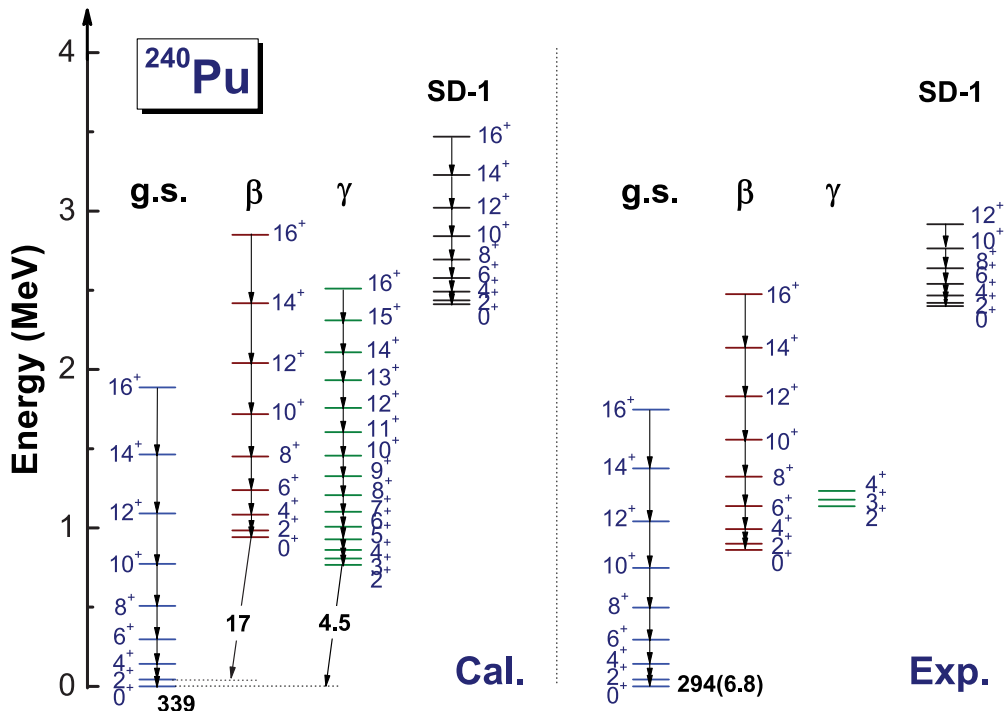

FIG. 3. (Color online) (left) Low-energy spectrum of ^{240}Pu calculated with the DD-PC1 relativistic density functional, compared with (right) data for the three lowest positive-parity bands at normal deformation, and the lowest $\pi = +$ superdeformed band.

well-known fact that the IB formula (20) predicts effective moments of inertia that are smaller than empirical values. More realistic values are only obtained if one uses the Thouless-Valatin (TV) formula. Here we rather follow the prescription of Ref. [20] where, by comparing the TV and IB moments of inertia as functions of the axial deformation for superdeformed bands in the $A = 190$–198 mass region, it was shown that the Thouless-Valatin correction to the perturbative expression IB is almost independent of deformation and does not include significant new structures in the moments of inertia. It was thus suggested that the moments of inertia to be used in the collective Hamiltonian can be simply related to the IB values through the minimal prescription $\mathcal{I}_k(q) = \mathcal{I}_k^{\text{IB}}(q)(1 + \alpha)$, where q denotes the generic deformation parameter and α is a constant that can be determined in a comparison with data. In the present study, $\alpha = 0.32$ for ^{240}Pu.

When the IB effective moment of inertia is renormalized to the empirical value, the excitation spectrum of the collective Hamiltonian determined by the functional DD-PC1 is in very good agreement with the available data for the ground-state band, β and γ bands, and even the lowest superdeformed band SD-1. Compared to the corresponding experimental sequence, the position of the γ band is predicted at somewhat lower excitation energy, and this might indicate that the theoretical PES is probably too soft in γ. The β band is calculated at slightly higher energy compared to experiment, and the predicted position of SD-1 is within the experimental error bounds. Very few data are available on electromagnetic transition rates in ^{240}Pu. In fact, except for the lifetime of the 2_1^+ state, only lifetimes of K isomers have been measured, but these include configurations not contained in our collective model space. Therefore, in Fig. 3 we only display the calculated $B(E2)$ values, in Weisskopf units (W.u.), for the transition $2_1^+ \rightarrow 0_1^+$ and from the bandheads of the β and γ bands to the ground-state band. We emphasize that, in addition to the renormalization of the moment of inertia, the calculation is completely parameter-free; that is, by using structure models based on self-consistent mean-field single-particle solutions, physical observables, such as transition probabilities and spectroscopic quadrupole moments, are calculated in the full configuration space and there is no need for effective charges. Using the bare value of the proton charge in the electric quadrupole operator $\hat{\mathcal{M}}(E2)$, the transition probabilities between eigenstates of the collective Hamiltonian can be directly compared to data.

B. γ-Vibrational bands in ^{166}Er

^{166}Er presents one of the best studied cases of mixing between the ground-state band and a low-lying γ band [32]. A marked feature of the excitation spectra of nuclei in this mass region is a low-energy $K^\pi = 2^+$ sequence of states, connected to the ground-state band by rather strong $E2$ transitions. It is interpreted as a γ-vibrational band, and the low excitation energy at which it occurs indicates a softness of the potential with respect to γ deformations.

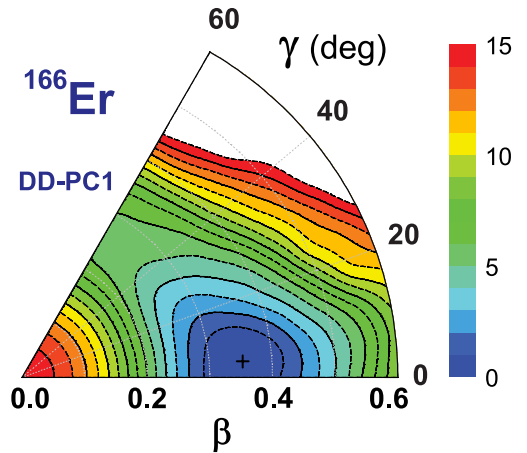The PES of ^{166}Er, obtained by constrained triaxial RHB calculations using the DD-PC1 energy density functional plus

FIG. 4. (Color online) Same as described in the caption of Fig. 1 but for the nucleus ^{166}Er.

the pairing interaction Eq. (12), is shown in Fig. 4. The minimum is calculated at $\beta = 0.35$ and $\gamma = 6°$ (i.e., the calculation predicts a slight deviation from axial symmetry, at least on the mean-field level). In the region of the minimum one might also notice that the calculated PES is soft in the γ direction but, as shown below, not soft enough to quantitatively reproduce the excitation of γ vibrations. The microscopic PES determines the deformation-dependent parameters of the quadrupole collective Hamiltonian, and the resulting low-energy spectrum is shown in Fig. 5 in comparison with data [33] for the ground-state band, the γ band, and the two-phonon γ-vibrational states $K^\pi = 4^+$ and 0^+. Namely, if the lowest $K^\pi = 2^+$ sequence is interpreted as a rotational band arising from the excitation of a quadrupole collective one-phonon γ vibration, one also expects to observe bands based on double (two-phonon) γ vibrations. Two intrinsic $K^\pi = 2^+$ quanta can be aligned parallel ($K^\pi = 4^+$) or antiparallel ($K^\pi = 0^+$). The observation of two-phonon vibrational states in deformed nuclei is more difficult than in spherical nuclei, also because of possible mixing with noncollective two-quasiparticle states and the resulting fragmentation of the vibrational strength. Nevertheless, evidence for two-phonon vibrational states in this region of well-deformed nuclei was reported in a number of experiments and, in particular for ^{166}Er, the $K^\pi = 4^+$ and $K^\pi = 0^+$ double γ-vibrational states were identified at 2028 and 1943 keV, respectively [34,35]. The measured $B(E2)$ values from these states to the bandhead of the γ band, $B(E2; 4_{\gamma\gamma}^+ \rightarrow 2_\gamma^+) = 8(3)$ W.u. and $B(E2; 0_{\gamma\gamma}^+ \rightarrow 2_\gamma^+) = 21(7)$ W.u. [33], show evidence of collective enhancement.

The relative position of two-phonon γ-vibrational states with respect to the corresponding one-phonon state provides information about the γ dependence of the potential [36], that is, whether the observed oscillation of the nuclear shape is with respect to an axially symmetric equilibrium, or if the nuclear equilibrium shape deviates from axial symmetry. In the former case (i.e., for harmonic γ vibrations around an axially symmetric shape), the $K^\pi = 4^+$ and $K^\pi = 0^+$ double γ-vibrational bandheads should occur at an energy of about
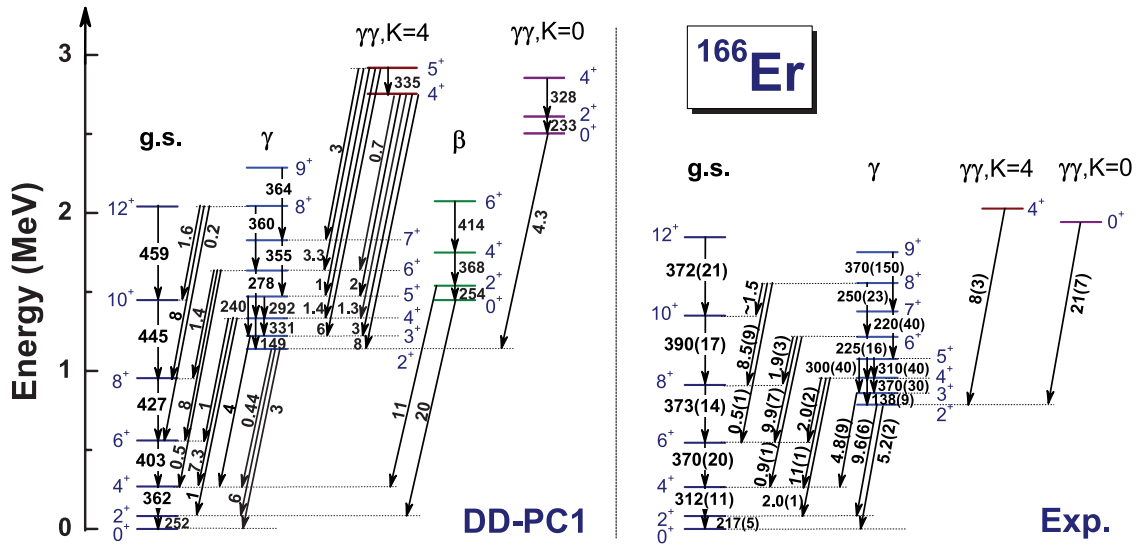
FIG. 5. (Color online) (left) Low-energy spectrum of ^{166}Er calculated with the DD-PC1 relativistic density functional compared with (right) data for the ground-state band, the γ band, and the two-phonon γ-vibrational states $K^\pi = 4^+$ and 0^+.

$2\hbar\omega = 2E_{2_\gamma^+}$. In the case of ^{166}Er, however,

$$R_{K=4} \equiv \frac{E(I = 4^+, K = 4)}{E(I = 2^+, K = 2)} = 2.58 \quad \text{and}$$

$$R_{K=0} \equiv \frac{E(I = 0^+, K = 0)}{E(I = 2^+, K = 2)} = 2.47$$

show significant deviation from harmonic vibrations and indicate that the potential surface might have a minimum for $\gamma \neq 0$.

After adjusting the Inglis-Belyaev moments of inertia to reproduce the energy of the first excited 2^+ state ($\alpha = 0.07$), as described in the previous subsection, we find a fair agreement between theory and experiment for the spectrum of ^{166}Er, especially the ground-state band and the γ band. In particular, the calculation reproduces the empirical $E2$ decay pattern, for both interband and intraband transitions, thus supporting the interpretation of the sequence of states built on the 2^+ state at 786 keV as a rotational band based on the one-phonon γ-vibrational state (see also Table II). One might notice that, with increasing angular momentum, the calculated $B(E2)$ values for transitions within the ground-state band and the γ band are systematically larger than the experimental values. This is because the theoretical states are purely collective, whereas experimental states in general include quasiparticle configurations and this mixing, not taken into account in our model space, reduces the collective enhancement of quadrupole transitions. The model also predicts rotational bands based on the double γ vibration: $K^\pi = 4^+$ and $K^\pi = 0^+$. The calculated $B(E2)$ for the transitions to the bandhead of the γ band, $B(E2; 4_{\gamma\gamma}^+ \to 2_\gamma^+) = 8.1$ W.u., is in excellent agreement with the experimental value of 8(3) W.u., and the predicted $B(E2; 0_{\gamma\gamma}^+ \to 2_\gamma^+) = 4.3$ W.u. is approximately five times smaller than the measured value of 21(7) W.u.

An obvious deficiency of the calculated excitation spectrum is the predicted positions of the γ bandhead at 1.14 MeV, that is, more than 300 keV above the experimental excitation

energy of the state 2_γ^+ and, correspondingly, the bandheads of the two-phonon γ bands: $K^\pi = 4^+$ at 2.75 MeV and $K^\pi = 0^+$ at 2.50 MeV. The γ-vibrational states are predicted at too-high excitation energies, and this might indicate that the theoretical PES is too stiff in γ and/or it could be a consequence of the cranking approximation used in the calculation of the mass parameters (vibrational inertial functions) [cf. Eqs. (21) and (22)]. Namely, as explained in the previous subsection, the missing Thouless-Valatin dynamical rearrangement contributions are approximately included in the moments of inertia by scaling the Inglis-Belyaev values by a common factor. The situation is considerably more complicated in the case of mass parameters [37,38], for which there are no simple estimates of the Thouless-Valatin correction, especially for nuclei with γ-soft potential energy surfaces. Some authors [38] have argued that, to approximately take into account the Thouless-Valatin correction, all inertial functions, and not only the moments of inertia, should be rescaled by a constant multiplicative factor. Because in the present analysis we are more interested in testing the predictions of the DD-PC1 energy density functional than in adjusting parameters to fit experimental spectra, such a rescaling of mass parameters was not attempted. It is worth noting, however, that the predicted ratios of excitation energies of two-phonon to one-phonon states, $R_{K=4} = 2.42$ and $R_{K=0} = 2.20$, correspond to anharmonic γ vibrations, as expected from the PES shown in Fig. 4. The corresponding empirical values, 2.58 and 2.47, respectively, are larger and show that γ anharmonicities in ^{166}Er are more pronounced.

The calculation also predicts a collective β band connected with large $E2$ transitions to the ground-state band: $B(E2; 0_\beta^+ \to 2_1^+) = 20$ W.u. and $B(E2; 2_\beta^+ \to 4_1^+) = 11$ W.u. The $B(E2)$ values for transitions within the β band are almost identical to those in the ground-state band. On the experimental side, the first and second excited 0^+ states, 0_2^+ at 1460 keV and 0_3^+ at 1713 keV, have small $B(E2)$ values for both the ground-state band and the γ band. In

TABLE II. $B(E2)$ values (in Weisskopf units) for transitions between low-energy states in ^{166}Er. Values calculated using the functionals DD-PC1 and PC-F1 are compared with available data [33].

J_i^π	J_f^π	DD-PC1	PC-F1	Expt.	J_i^π	J_f^π	DD-PC1	PC-F1	Expt.
$2^+_{g.s.}$	$0^+_{g.s.}$	252	253	217(5)	8^+_γ	$6^+_{g.s.}$	0.16	0.001	0.52(5)
$4^+_{g.s.}$	$2^+_{g.s.}$	362	367	312(11)		$8^+_{g.s.}$	7.9	12.1	8.5(9)
$6^+_{g.s.}$	$4^+_{g.s.}$	403	413	370(20)		$10^+_{g.s.}$	1.6	0.5	~1.5
$8^+_{g.s.}$	$6^+_{g.s.}$	427	444	373(14)		6^+_γ	361	359	250(23)
$10^+_{g.s.}$	$8^+_{g.s.}$	445	470	390(17)	9^+_γ	7^+_γ	384	385	370(150)
$12^+_{g.s.}$	$10^+_{g.s.}$	459	493	372(21)					
					$4^+_{\gamma\gamma,4}$	2^+_γ	8.1	7.5	8(3)
2^+_γ	$0^+_{g.s.}$	3.04	3.36	5.17(21)		3^+_γ	2.8	9.6	
	$2^+_{g.s.}$	5.9	8.0	9.6(6)		4^+_γ	1.3	5.6	
	$4^+_{g.s.}$	0.4	0.4			5^+_γ	1.8	0.2	
3^+_γ	$2^+_{g.s.}$	5.5	6.4			6^+_γ	0.7	0.1	
	$4^+_{g.s.}$	3.9	5.4	4.8(9)	$5^+_{\gamma\gamma,4}$	3^+_γ	6.4	3.2	
	2^+_γ	444	414			4^+_γ	1.4	9.7	
4^+_γ	$2^+_{g.s.}$	1.08	0.77	1.98(12)		5^+_γ	1.1	8.1	
	$4^+_{g.s.}$	7.3	10.4	11.1(7)		6^+_γ	3.3	1.4	
	$6^+_{g.s.}$	1.03	0.78	2.01(14)		7^+_γ	3.1	0.1	
	2^+_γ	149	141	138(9)		$4^+_{\gamma\gamma,4}$	335	315	
	3^+_γ	331	310	370(30)					
5^+_γ	$4^+_{g.s.}$	7.3	4.3	8.9(11)	0^+_β	$2^+_{g.s.}$	20.1	30.9	8.8(9)
	$6^+_{g.s.}$	5.6	7.5	12.4(15)	2^+_β	$4^+_{g.s.}$	11.2	18.7	
	3^+_γ	240	230	300(40)		0^+_β	255	245	
	4^+_γ	239	222	310(40)	4^+_β	2^+_β	368	359	
6^+_γ	$4^+_{g.s.}$	0.45	0.14	0.88(6)	6^+_β	4^+_β	414	411	
	$6^+_{g.s.}$	7.7	11.4	9.9(7)					
	$8^+_{g.s.}$	1.4	0.7	1.9(3)	$0^+_{\gamma\gamma,0}$	2^+_γ	4.3	10.7	21(7)
	4^+_γ	296	288	225(16)	$2^+_{\gamma\gamma,0}$	$0^+_{\gamma\gamma,0}$	233	174	
7^+_γ	$6^+_{g.s.}$	3.0	3.0	3.4(7)	$4^+_{\gamma\gamma,0}$	$2^+_{\gamma\gamma,0}$	328	251	
	$8^+_{g.s.}$	6.7	8.9	8.0(16)					
	5^+_γ	335	329	220(40)					

addition, these two states are relatively strongly populated in two-neutron transfer reactions and, therefore, are identified as predominantly pair-type excitations. For the 0^+_4 at 1934 keV, the measured $B(E2)$ value for the transition $0^+_4 \to 2^+_1$ is 8.8 (9) W.u. and, together with its population in two-neutron transfer, suggests that it can be identified as a β-vibrational state [39]. Therefore, the only excited 0^+ state that displays a collective enhancement of the decay to the ground-state band is located far above the predicted position of the β-vibrational band. Qualitatively, this can be understood as owing to the mixing with other excited 0^+ states, not included in the model space. The excited 0^+ states are also very sensitive to the coupling of nuclear shape oscillations to pairing vibrations (i.e., vibrations of the pairing density), but this effect is not considered in our model of quadrupole dynamics.

To examine quantitatively how the softness of microscopic potentials affects γ vibrations, we performed another set of constrained RHB plus collective Hamiltonian calculations, using a different energy density functional: PC-F1 [40]. The
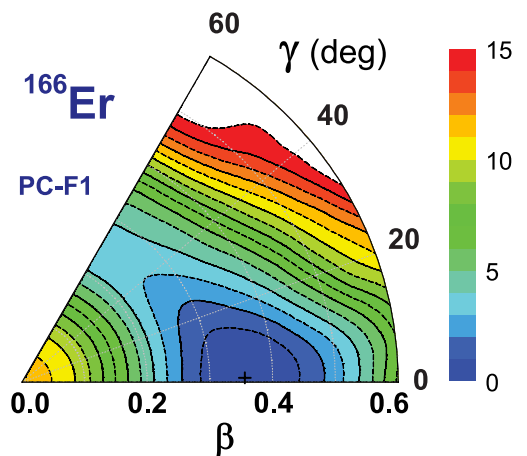

FIG. 6. (Color online) Same as described in the caption of Fig. 1 but for the binding energy map of the nucleus ^{166}Er calculated using the energy density functional PC-F1.
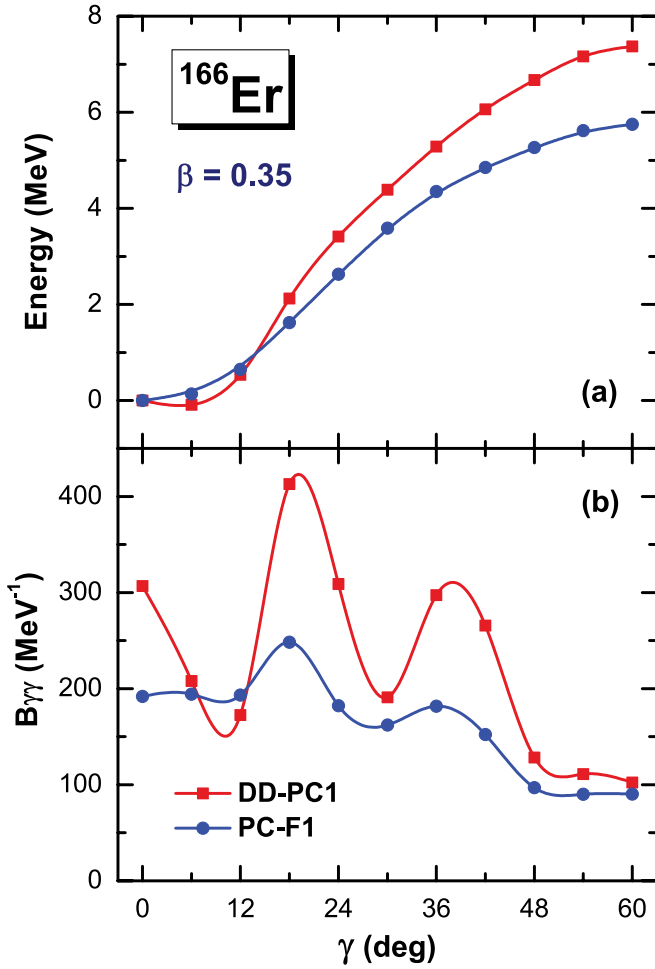
FIG. 7. (Color online) (a) Self-consistent RHB binding energy curves and (b) cranking mass parameters $B_{\gamma\gamma}$ of ^{166}Er at the axial deformation $\beta = 0.35$, calculated with the energy density functionals DD-PC1 and PC-F1, as functions of the deformation parameter γ.

relativistic functional PC-F1 was adjusted to ground-state observables (binding energies, charge radii, diffraction radii, and surface thickness) of spherical nuclei and tested in the analysis of the equation of state of symmetric nuclear matter and neutron matter, binding energies and form factors, and ground-state properties of several isotopic and isotonic chains. We also used this functional in our previous multireference calculations, including the generator coordinate method in Refs. [7,8] and the five-dimensional collective Hamiltonian [9,41–43]. Figure 6 displays the triaxial PES of ^{166}Er, calculated in the RHB model using the energy density functional PC-F1 plus the pairing interaction Eq. (12). Comparing with the corresponding PES calculated with DD-PC1 (cf. Fig. 4) one notes that in this case the minimum is on the prolate axis: $\beta \approx 0.35$ and $\gamma = 0$, and that the potential is softer with respect to γ deformations. This is shown more clearly in Fig. 7(a), where we plot the γ dependence of the two PESs in the region of the prolate minimum (i.e., the DD-PC1 and PC-F1 binding energy curves at the axial deformation $\beta = 0.35$), as functions of the deformation parameter γ. The minimum of the DD-PC1 PES is at $\gamma = 6°$, whereas PC-F1 predicts an axially symmetric mean-field minimum. The PES calculated with PC-F1 is considerably softer in the γ direction. The two functionals also predict different inertia parameters. Figure 7(b) displays the γ dependence of the corresponding mass parameters $B_{\gamma\gamma}$, calculated at the axial deformation $\beta = 0.35$. Both functionals predict an oscillatory γ dependence of $B_{\gamma\gamma}$, but the amplitudes and the average value calculated with DD-PC1 are considerably larger. The differences in the PES and mass parameters are reflected in the corresponding spectrum, as shown in Fig. 8.

The excitation spectrum predicted by the PC-F1 energy density functional is not very different from the one obtained with DD-PC1 (cf. Fig. 5) but, because the PES is slightly softer with respect to γ deformation, the one-phonon and two-phonon γ bands are calculated at lower energies, apparently in
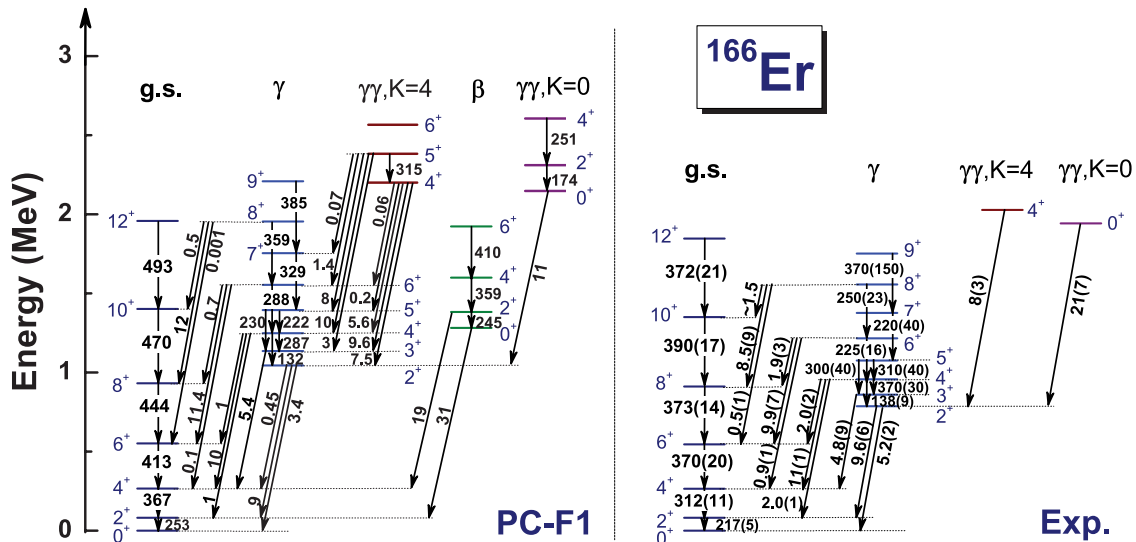

FIG. 8. (Color online) Same as described in the caption of Fig. 5 but the collective spectrum of ^{166}Er is calculated using the energy density functional PC-F1.

better agreement with experiment. The state 2_γ^+ is lowered by ≈ 100 keV, and the two-phonon states are lowered by as much as 500 keV. One might also notice that the calculated $4_{\gamma\gamma}^+$ and $0_{\gamma\gamma}^+$ are almost degenerate, in accord with the corresponding experimental levels. However, because the PES of PC-F1 is harmonic in γ in the region of the prolate minimum, the resulting excitation spectrum is much closer to the harmonic limit; that is, $R_{K=4} = 2.11$ and $R_{K=0} = 2.06$. Thus, the stiff and γ-anharmonic PES of DD-PC1 predicts a γ-vibrational spectrum that has too-large $\hbar\omega$ but displays an anharmonicity close to the empirical one, whereas the softer and γ-harmonic PES of PC-F1 leads to an almost harmonic γ-vibrational spectrum with a more realistic $\hbar\omega$. We also note that the $BE(2)$ values calculated with PC-F1 are on the same level of agreement with data as those obtained with DD-PC1 (cf. Table II) and, in some cases, even better. For instance, PC-F1 predicts the value $B(E2; 0_{\gamma\gamma}^+ \to 2_\gamma^+) = 10.7$ W.u., closer to the empirical value of 21(7) W.u., and the same is true for virtually all transitions from the γ band to the ground-state band.

Finally, the level of mixing of $K = 0$ and $K = 2$ components in the wave functions is reflected in the staggering in energy between odd- and even-spin states in the γ band. The staggering can be quantified by considering the differential quantity [44]

$$S(J)$$
$$= \frac{\{E[J_\gamma^+] - E[(J-1)_\gamma^+]\} - \{E[(J-1)_\gamma^+] - E[(J-2)_\gamma^+]\}}{E[2_1^+]},$$
(29)

which characterizes the displacement of the $(J-1)_\gamma^+$ level relative to the average of its neighbors, J_γ^+ and $(J-2)_\gamma^+$, normalized to the energy of the first excited state of the ground-state band, 2_1^+. For a spectrum of a pure rotor, $S(J)$ is constant, that is, 0.333. In Fig. 9 we plot the angular momentum dependence of $S(J)$ calculated with the functionals DD-PC1 and PC-F1 (cf. Figs. 5 and 8) in comparison with
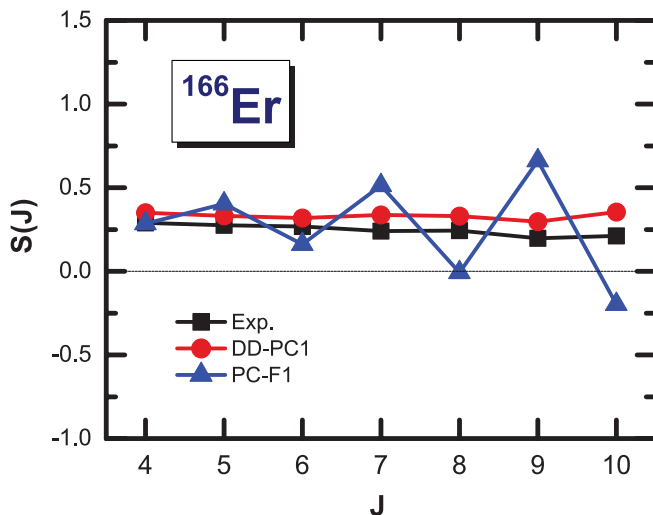

FIG. 9. (Color online) Staggering $S(J)$ defined in Eq. (29) for the γ band of ^{166}Er. The results calculated with the density functionals DD-PC1 and PC-F1 are compared with data.

the experimental values. The calculation with DD-PC1 nicely reproduces the almost constant empirical behavior of $S(J)$ in ^{166}Er, whereas PC-F1 predicts a pronounced staggering with smaller values for even-spin states and larger values for odd-spin states, and the magnitude increases with spin. This behavior is characteristic for a transitional γ-soft potential [45] but, obviously, is not in agreement with data.

V. CONCLUSIONS

Prompted by a wealth of new experimental results in exotic nuclei far from β stability, and by theoretical developments in related fields, important advances have been made in recent years in building the framework of NEDFs, the tool of choice for a consistent microscopic description of medium-heavy and heavy nuclei.

Different approaches, some complementary, have characterized the development of NEDFs, with the result that at present many global functionals, in both nonrelativistic and relativistic frameworks, are used in nuclear structure studies. This means, however, that it is often difficult to compare results obtained with different models, also because they include different subsets of terms from a general functional that can be expressed in terms of powers and gradients of ground-state nucleon densities and currents. It is, therefore, important to perform detailed tests of the predictions of various functionals in comparison with spectroscopic data. Most modern energy density functionals, and in particular the relativistic ones, have only been used in single-reference calculations (i.e., in self-consistent mean-field calculations of ground-state properties) and, eventually, in studies of giant resonances using the (quasiparticle) random-phase approximation. However, to be able to make detailed predictions for excitation spectra and electromagnetic transition probabilities, correlations beyond the static mean field must be included through restoration of broken symmetries, and configuration mixing of symmetry-breaking product states must be taken into account.

In this work we presented a study of low-energy collective spectra of two nuclei, ^{166}Er and ^{240}Pu, using the recently introduced relativistic density functional DD-PC1. Starting from microscopic nucleon self-energies in nuclear matter, the parameters of this functional were determined exclusively from a fit to binding energies of a set of 64 axially deformed nuclei in the mass regions $A \approx 150$–180 and $A \approx 230$–250. DD-PC1 was previously tested in calculations of ground-state properties and excitation energies of giant multipole resonances, but this is the first application in a study of low-energy excitation spectra. The framework used in the present study includes the three-dimensional relativistic Hartree-Bogoliubov model with a separable pairing force and the model for the solution of a collective Hamiltonian in five dimensions for quadrupole vibrational and rotational degrees of freedom.

The relativistic Hartree-Bogoliubov model, with the functional DD-PC1 in the particle-hole channel and a separable pairing force in the particle-particle channel, is used to perform constrained self-consistent triaxial calculations of binding energy maps as functions of quadrupole deformation in the β-γ

plane. The resulting single-quasiparticle energies and wave functions provide the microscopic input for the parameters of the collective Hamiltonian for vibrations and rotations: the mass parameters, the moments of inertia, and the collective potential. The solution of the corresponding eigenvalue problem yields the excitation spectra and collective wave functions that are used in the calculation of electromagnetic transition probabilities.

The nuclei ^{166}Er and ^{240}Pu were chosen as representative of the two mass regions in which the parameters of DD-PC1 have been adjusted to binding energies. For both systems, the present study showed good agreement with data on low-energy positive-parity collective states. In the case of ^{240}Pu, the RHB calculation reproduces the experimental values for the ground-state deformation, the barrier height, and the excitation energy of the second minimum. The inclusion of triaxial shapes, in particular, lowers the inner barrier by ≈ 2 MeV, in agreement with data. The excitation spectrum of the collective Hamiltonian determined by the functional DD-PC1 reproduces the available data for the ground-state band, β and γ bands, and the lowest superdeformed band SD-1. ^{166}Er presents a nice example for studies of the mixing between the ground-state band and a low-lying γ band, and available data on two-phonon γ-vibrational states provide information about the stiffness and anharmonicity of the collective potential energy surface. The results of the diagonalization of the collective Hamiltonian are in good agreement with experiment, especially the spectra of the ground-state band and the γ band, the staggering of the γ band, and the pattern of $E2$ interband and intraband transitions. The model also predicts rotational bands based on the double γ vibration and reproduces the $B(E2)$ values for transitions to the bandhead of the γ band. It seems, however, that DD-PC1 predicts a collective potential that is too stiff with respect to γ deformation, with the result that the calculated one- and two-phonon states are located at higher excitation energies compared with the corresponding experimental levels. The DD-PC1 PES of ^{166}Er has a minimum at $\gamma \neq 0$, and this leads to a γ-anharmonic spectrum with a level of anharmonicity close to the empirical one.

The tests performed in Ref. [6] and the present investigation have shown that the relativistic energy density functional DD-PC1, adjusted exclusively to masses of axially deformed heavy nuclei, not only reproduces ground-state properties and excitation energies of giant resonances in "mean-field level" calculations but, when used as a microscopic input for the collective Hamiltonian, also provides a quantitative description of complex excitation spectra and electromagnetic transition patterns. Therefore, we plan to employ DD-PC1

in systematic studies of low-energy collective spectroscopy, especially shape coexistence and shape transition phenomena in medium-heavy and heavy nuclei, using either the generator coordinate method for configuration mixing of angular momentum projected triaxial mean-field wave functions [10,46], or the collective Hamiltonian in five dimensions for quadrupole vibrational and rotational degrees of freedom [9]. It must be emphasized, however, that those correlations that we wish to treat explicitly as, for instance, rotational energy corrections and quadrupole fluctuations should not already be included in the energy functional in an implicit way. This is, of course, the case with all modern functionals, including also DD-PC1, that have been adjusted directly to experimental masses and/or radii. The solution would be to readjust a given functional to pseudodata, obtained by subtracting correlation effects from data (experimental masses and, eventually, radii). Approximate methods for the calculation of correlations have been developed [47] that will enable a systematic evaluation of correlation energies for the nuclear mass table. In the case of DD-PC1, the subtraction of correlation energies from experimental masses leads to a fine tuning of the coupling constants but, of course, we do not expect significant changes in the parameters.

A very important additional test of this framework is a detailed investigation of the structure of even-even nuclei at normal deformation, in comparison with results obtained in the recent global study based on the nonrelativistic Hartree-Fock-Bogoliubov framework with the Gogny interaction D1S and mapped onto a five-dimensional collective quadrupole Hamiltonian [48]. Finally, it would be equally important to connect the semiempirical DD-PC1 more directly with energy density functionals based on a fully microscopic approach to symmetric and asymmetric nucleonic matter [4,5].

[1] M. Bender, P.-H. Heenen, and P.-G. Reinhard, Rev. Mod. Phys. **75**, 121 (2003).

[2] G. A. Lalazissis, P. Ring, and D. Vretenar (Eds.), *Extended Density Functionals in Nuclear Structure Physics*, Lecture Notes in Physics Vol. 641 (Springer, Heidelberg, 2004).

[3] J. E. Drut, R. J. Furnstahl, and L. Platter, Prog. Part. Nucl. Phys. **64**, 120 (2010).

[4] P. Finelli, N. Kaiser, D. Vretenar, and W. Weise, Nucl. Phys. A **770**, 1 (2006).

[5] D. Vretenar, Eur. Phys. J. Spec. Top. **156**, 37 (2008).

[6] T. Nikšić, D. Vretenar, and P. Ring, Phys. Rev. C **78**, 034318 (2008).

[7] T. Nikšić, D. Vretenar, and P. Ring, Phys. Rev. C **73**, 034308 (2006).

[8] T. Nikšić, D. Vretenar, and P. Ring, Phys. Rev. C **74**, 064309 (2006).

[9] T. Nikšić, Z. P. Li, D. Vretenar, L. Próchniak, J. Meng, and P. Ring, Phys. Rev. C **79**, 034303 (2009).

[10] J. M. Yao, J. Meng, P. Ring, and D. Pena Arteaga, Phys. Rev. C **79**, 044312 (2009).

[11] D. Vretenar, A. V. Afanasjev, G. A. Lalazissis, and P. Ring, Phys. Rep. **409**, 101 (2005).

[12] J. Meng, Nucl. Phys. A **635**, 3 (1998).

[13] J. Meng, H. Toki, S. G. Zhou, S. Q. Zhang, W. H. Long, and L. S. Geng, Prog. Part. Nucl. Phys. **57**, 470 (2006).

[14] Y. Tian, Z. Y. Ma, and P. Ring, Phys. Lett. B **676**, 44 (2009).

[15] Y. Tian, Z. Y. Ma, and P. Ring, Phys. Rev. C **79**, 064301 (2009).

[16] Y. Tian, Z. Y. Ma, and P. Ring, Phys. Rev. C **80**, 024313 (2009).

[17] J. F. Berger, M. Girod, and D. Gogny, Comput. Phys. Commun. **63**, 365 (1991).

[18] P. Ring and P. Schuck, *The Nuclear Many-Body Problem* (Springer-Verlag, Heidelberg, 1980).

[19] K. Kumar and M. Baranger, Nucl. Phys. A **92**, 608 (1967).

[20] J. Libert, M. Girod, and J.-P. Delaroche, Phys. Rev. C **60**, 054301 (1999).

[21] T. Bürvenich, M. Bender, J. A. Maruhn, and P.-G. Reinhard, Phys. Rev. C **69**, 014307 (2004).

[22] L. Bonneau, P. Quentin, and D. Samsoen, Eur. Phys. J. A **21**, 391 (2004).

[23] H.-F. Lü, L.-S. Geng, and J. Meng, Chin. Phys. Lett. **23**, 2940 (2006).

[24] M. Girod, J. Libert, J.-P. Delaroche, and P. Romain, Eur. Phys. J. A **15**, 209 (2002).

[25] M. Bender, P.-H. Heenen, and P. Bonche, Phys. Rev. C **70**, 054304 (2004).

[26] J.-P. Delaroche, M. Girod, H. Goutte, and J. Libert, Nucl. Phys. A **771**, 103 (2006).

[27] L. Próchniak, Int. J. Mod. Phys. E **17**, 160 (2008).

[28] S. Bjørnholm and J. E. Lynn, Rev. Mod. Phys. **52**, 725 (1980).

[29] R. B. Firestone, V. S. Shirley, S. Y. F. Chu, C. M. Baglin, and J. Zipkin, *Table of Isotopes* (Wiley, New York, 1996).

[30] K. E. G. Löbner, M. Vetter, and V. Hönig, Nucl. Data Tables A **7**, 495 (1970).

[31] C. E. Bemis Jr., F. K. McGowan, J. L. C. Ford Jr., W. T. Milner, P. H. Stelson, and R. L. Robinson, Phys. Rev. C **8**, 1466 (1973).

[32] A. Bohr and B. R. Mottelson, *Nuclear Structure*, Vol. II (Benjamin, Reading, PA, 1975).

[33] C. M. Baglin, Nucl. Data Sheets **109**, 1103 (2008).

[34] C. Fahlander, A. Axelsson, M. Heinebrodt, T. Härtlein, and D. Schwalm, Phys. Lett. B **388**, 475 (1996).

[35] P. E. Garrett, M. Kadi, Min Li, C. A. McGrath, V. Sorokin, M. Yeh, and S. W. Yates, Phys. Rev. Lett. **78**, 4545 (1997).

[36] A. Bohr and B. R. Mottelson, Phys. Scr. **25**, 28 (1982).

[37] L. Próchniak, P. Quentin, D. Samsoen, and J. Libert, Nucl. Phys. A **730**, 59 (2004).

[38] L. Próchniak and S. G. Rohoziński, J. Phys. G **36**, 123101 (2009).

[39] P. E. Garrett, M. Kadi, C. A. McGrath, V. Sorokin, M. Li, M. Yeh, and S. W. Yates, Phys. Lett. B **400**, 250 (1997).

[40] T. Bürvenich, D. G. Madland, J. A. Maruhn, and P.-G. Reinhard, Phys. Rev. C **65**, 044308 (2002).

[41] Z. P. Li, T. Nikšić, D. Vretenar, J. Meng, G. A. Lalazissis, and P. Ring, Phys. Rev. C **79**, 054301 (2009).

[42] Z. P. Li, T. Nikšić, D. Vretenar, and J. Meng, Phys. Rev. C **80**, 061301(R) (2009).

[43] Z. P. Li, T. Nikšić, D. Vretenar, and J. Meng, Phys. Rev. C **81**, 034316 (2010).

[44] N. Zamfir and R. Casten, Phys. Lett. B **260**, 265 (1991).

[45] E. A. McCutchan, D. Bonatsos, N. V. Zamfir, and R. F. Casten, Phys. Rev. C **76**, 024306 (2007).

[46] J. M. Yao, J. Meng, P. Ring, and D. Vretenar, Phys. Rev. C **81**, 044311 (2010).

[47] M. Bender, G. F. Bertsch, and P.-H. Heenen, Phys. Rev. C **69**, 034340 (2004).

[48] J.-P. Delaroche, M. Girod, J. Libert, H. Goutte, S. Hilaire, S. Péru, N. Pillet, and G. F. Bertsch, Phys. Rev. C **81**, 014303 (2010).